Internal dynamics of multilevel atoms near a vacuum-dielectric interface

J.-Y. Courtois
Institut d'Optique Théorique et Appliquée, Boîte Postale 147, F-91403 Orsay Cedex, France

J.-M. Courty
Laboratoire Kastler-Brossel, Case 74, Université Pierre et Marie Curie, Ecole Normale Supérieure, CNRS, F-75252 Paris Cedex 05, France

J. C. Mertz
School of Applied and Engineering Physics, Cornell University, Ithaca, New York 14853
(Received 20 September 1995)

We show how the internal dynamics of a multilevel atom are modified in the vicinity of the interface between a vacuum and a simple or multilayered lossless dielectric medium. Optical Bloch equations are derived, which take into account the modifications of spontaneous emission rates and energy levels experienced by the atom. van der Waals level shifts are evaluated using the method of images for dielectrics. Spontaneous emission rates and radiation patterns are calculated in a simple way using the Lorentz reciprocity theorem.

PACS number(s): 42.50.Ct, 31.30.Jv, 03.65.Sq, 32.70.Jz

I. INTRODUCTION

The electromagnetic field surrounding an atom becomes modified when the atom is located close to a surface. It has been known theoretically for many years that this affects the radiation properties of the atom. In particular, the presence of the surface changes the natural lifetime and the energy of the atomic levels, as well as the spontaneous emission radiation distribution. Recent experimental investigations in selective reflection spectroscopy at an interface between a dielectric and a dilute vapor of alkali atoms [1] have occasioned a renewed interest in these effects. From a different standpoint, the development of atomic mirrors in atomic optics [2] has drawn attention to so-called evanescent wave mirrors [3] (obtained by total internal reflection of a laser beam at the interface between a vacuum and a dielectric medium), particularly following the recent experimental demonstration of evanescent field enhancement by means of surface plasmons [4] or thin dielectric waveguides [5]. Both experimental situations (reflection spectroscopy and evanescent wave mirrors) involve the interaction of multilevel atoms with light at distances from a vacuum-dielectric interface which are smaller than or comparable to the optical wavelength. Under such conditions, it is no longer legitimate to neglect the influence of the interface on the atomic dynamics. An evaluation of this influence is, therefore, timely.

In the present introductory study of the optical Bloch equations for a multilevel atom near a vacuum-dielectric interface, we consider a simple model which can be explicitly dealt with by elementary calculations. The simplest situation is that of an infinite space which is filled below the plane $z=0$ with one or several layers of nonmagnetic, transparent, homogeneous, isotropic media of widths l_i and refractive indices n_i (dielectric constant $\epsilon_i=n_i^2$), and which is empty everywhere above this plane (Fig. 1). In principle, the indices n_i must be considered as complex functions of the optical frequency ω. Indeed, it is well known that the causality requirement imposes constraints on the allowed form of $n_i(\omega)$, so that the real and imaginary parts of $n_i(\omega)-1$ are coupled by Hilbert transform dispersion relations [6]. However, we make the simplifying assumption that the imaginary parts of the refractive indices vanish over all frequencies up to and including the optical region which concerns us, and only become nonzero at much higher frequencies, say in the far UV. Under these assumptions, the real parts of the refractive indices are nearly constant over the frequencies of interest, and n_i can be treated as a real number. An atom is placed *in vacuo* a distance Z above the surface of the dielectric medium, where it interacts with a laser field of frequency ω_L. This laser is quasiresonant with a closed transition of the atom connecting its ground state $|g\rangle$ of angular momentum J_g to an excited state $|e\rangle$ of angular momentum J_e.

The paper is organized as follows. In Sec. II, we derive a general form of the optical Bloch equations characterizing the internal dynamics of a multilevel atom near a vacuum-dielectric interface. We show that the presence of the inter-

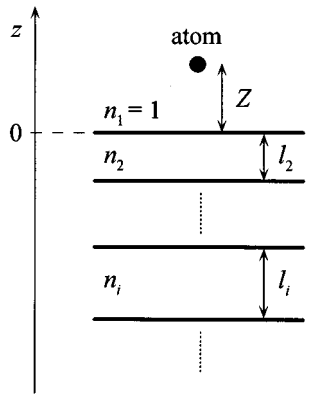

FIG. 1. Schematic representation of the model considered in this paper. An infinite space consists of a vacuum above the plane $z=0$, and one or more layers of dielectric media of widths l_i and refractive indices n_i below the plane $z=0$. An atom is placed a distance Z above the vacuum-dielectric interface.

face modifies the atom-field coupling in two distinct ways. First, the energy shifts of the atomic levels result in a space-dependent frequency detuning between the laser field and the atomic resonance frequencies. Second, the atomic relaxation associated with spontaneous emission is significantly modified. On the one hand, the interface breaks the isotropy of spontaneous emission and leads to different relaxation rates depending on the polarization of the atomic dipole moment. On the other hand, because of the loss of translation symmetry in the direction orthogonal to the dielectric surface, the spontaneous emission rates become space-dependent. In Sec. III, we describe more explicitly two situations of experimental interest in which multilevel alkali atoms are located close to a simple vacuum-dielectric interface, or to a multilayered dielectric waveguide. Using the method of images for dielectrics, we evaluate the shifts of the atomic levels in the limit of small distances from the interface, where they arise essentially from the van der Waals interaction between the atom and the dielectric medium. Finally, we derive in a simple and rigorous way the spontaneous emission rates as well as the radiation patterns for an atom at any distance from the interface, using Lorentz's reciprocity theorem.

II. OPTICAL BLOCH EQUATIONS

The internal dynamics of an atom interacting with a laser field are conveniently characterized by a master equation for its density matrix (optical Bloch equations). This section is devoted to the derivation of such an equation in the particular case where a multilevel atom is located close to the interface between a vacuum and a dielectric medium.

A. General

To begin, we identify the general features of the optical Bloch equations at an interface. In free space, the master equation describing the interaction of a single multilevel atom with a monochromatic laser field is well known [7]. Basically, its derivation proceeds in two steps. In the first step, one considers the evolution equation for the total density matrix of the system constituted by the atom and the electromagnetic field. In the framework of nonrelativistic quantum electrodynamics and in the electric dipole approximation, this equation relies upon the atom-field Hamiltonian

$$H = H_0 + H_R + V_{AL} + V_{AR}. \tag{1}$$

The first term on the right-hand side of Eq. (1) is the purely internal Hamiltonian describing the energy level structure of the *bare* atom

$$H_0 = \sum_i E_i |i\rangle\langle i|, \tag{2}$$

the index i being short for a complete set of internal quantum numbers (in the following, we will be mainly interested in the quantum numbers J and M, denoting, respectively, the magnitude and the z component of the total angular momentum); the second term is the free Hamiltonian of the Coulomb-gauge quantized electromagnetic field; V_{AL} is the time-dependent, purely atomic Hamiltonian

$$V_{AL}(t) = -\mathbf{D}\cdot\mathscr{E}_L(t), \tag{3}$$

which describes the interaction of the atomic dipole $\mathbf{D}$ with the laser field assumed to be in a coherent state and therefore described by a *classical* function $\mathscr{E}_L(t)$; and the last term,

$$V_{AR} = -\mathbf{D}\cdot\mathbf{E}, \tag{4}$$

represents the coupling between the atom and the reservoir associated with the vacuum quantum field $\mathbf{E}$. We note that in Eq. (1), both fields $\mathscr{E}_L(t)$ and $\mathbf{E}$ are evaluated at the location of the atom. In the second step, the master equation for the atomic density matrix ρ is obtained by applying second order perturbation theory to the atom-reservoir interaction, and by tracing away the degrees of freedom associated with the reservoir. This yields a dynamical evolution equation where the influence of the reservoir is manifest through two contributions. The first, associated with an effective Hamiltonian, describes the energy shifts undergone by the atomic levels as a result of their coupling to the vacuum field (Lamb shifts). These shifts are traditionally assimilated in the definition of H_0, yielding the actual internal Hamiltonian $H_{A,\infty}$. The second contribution, $\dot{\rho}_{relax,\infty}$, represents the dissipation of the atomic system due to its coupling with the reservoir (spontaneous emission). Finally, the free-space time evolution of the atomic density matrix takes the form

$$\dot{\rho} = \mathscr{L}_\infty \rho, \tag{5}$$

$$\mathscr{L}_\infty \rho = \frac{1}{i\hbar}[H_{A,\infty} + V_{AL}, \rho] + \dot{\rho}_{relax,\infty}, \tag{6}$$

where we have introduced the free-space Liouvillian superoperator $\mathscr{L}_\infty$.

We now consider an atom located in the vicinity of a vacuum-dielectric interface. What are the modifications of the master equation (5) induced by the lower-lying dielectric medium? First, because of the new boundary conditions, the modes of $\mathscr{E}_L(t)$ and of the quantized electromagnetic vacuum field are altered and may become evanescent. It is clear that this does not affect the operators H_0, H_R, and V_{AL}, which keep the same form as in the free-space case. In contrast, the structure of the reservoir becomes modified. The contributions of V_{AR} to the atom dynamics (energy level shifts and spontaneous emission rates) are therefore expected to be different from the free-space situation. Moreover, as a result of the instantaneous Coulomb interaction between the atomic and dielectric charges, one expects a supplementary electrostatic contribution H_{es} to the energy level shifts. H_{es} corresponds to the London–van der Waals interaction of the instantaneous atomic dipole with its image(s) in the dielectric medium. Higher multipoles can be neglected provided the atomic radius is much less than the distance between the atom and the dielectric surface (which will always be assumed in this paper). Finally, denoting by ΔH_A and $\dot{\rho}_{relax,int}$ the modifications of the Hamiltonian and dissipative parts of the atomic density matrix evolution due to the interface, one obtains the general form of the optical Bloch equations in the presence of the dielectric medium

$$\dot{\rho} = \mathscr{L}_\infty \rho + \mathscr{L}_{int}\rho, \tag{7}$$

where

$$\mathscr{L}_{int}\rho=\frac{1}{i\hbar}[\Delta H_A,\rho]+\dot{\rho}_{relax,int} \tag{8}$$

entirely describes the influence of the interface on the atomic internal dynamics. In particular, $\mathscr{L}_{int}\rho$ tends toward zero when the atom is far from the dielectric surface. We discuss the two contributions to Eq. (8) in more detail below.

B. General properties of the interface-induced energy-level shifts

We first consider the energy shifts undergone by the atomic levels due to the presence of the lower-lying dielectric medium. Our aim in this section is to describe some general properties of the level shifts, and to identify their contributions to the atomic dynamics. We defer the explicit expressions of these shifts to Sec. III, since they depend on the particular structure of the atom and of the dielectric medium.

As emphasized above, the interface-induced energy shift ΔE_i of level $|i\rangle$ results from the interaction Hamiltonian $H_{es}+V_{AR}$. One can thus distinguish two contributions to the atomic level shifts [8]

$$\Delta E_i=\Delta E_{es,i}+\Delta E_{AR,i}, \tag{9}$$

where $\Delta E_{es,i}$ arises from H_{es}, while $\Delta E_{AR,i}$ arises, in second-order perturbation theory, from V_{AR}. In particular, $\Delta E_{AR,i}$ embodies the effect analogous to the free-space Lamb shift. Because $\Delta E_{es,i}$ and $\Delta E_{AR,i}$ are defined relative to their corresponding values in free space (the latter being included in $H_{A,\infty}$), both contributions tend towards zero when the atom is far from the dielectric surface.

Let us now discuss the symmetry properties of the system under rotations of the internal atomic variables. First, there is a manifest invariance under rotations about the z axis. The z component of the total angular momentum M is therefore a good quantum number. Second, because of invariance under time reversal, the energy shifts can depend only on the magnitude, but not on the sign, of M. It then follows from the preceding considerations that the purely internal effective Hamiltonians ΔH_{es} and ΔH_{AR} associated with the energy shifts in Eq. (9), and hence the total Hamiltonian ΔH_A associated with these shifts, split into a scalar part $\Delta H_A^{(S)}$ and a quadrupolar part $\Delta H_A^{(Q)}$ [8]:

$$\Delta H_A=\Delta H_A^{(S)}+\Delta H_A^{(Q)}. \tag{10}$$

The scalar part $\Delta H_A^{(S)}$ shifts the atomic levels, but does not lift their Zeeman degeneracy, nor mix energy levels of different angular momenta J. The quadrupolar part $\Delta H_A^{(Q)}$, which transforms like Y_{20} under rotations, can in principle mix atomic levels of the same parity but different Js (provided they differ by at most 2). It turns out that as far as the fine structure of the atom is concerned, such a mixing is almost always negligible in experimental situations of interest (for a more detailed discussion, and for the case of hyperfine atomic levels, see Sec. III). One is therefore mainly concerned with the effect of $\Delta H_A^{(Q)}$ inside the Zeeman degeneracy subspace of a single atomic level, where $\Delta H_A^{(Q)}$ does not shift the net average of the Zeeman sublevels, and produces a splitting pattern which has the same symmetry as the Stark shifts that would be produced by a fictitious static electric field parallel to the z axis,

$$\Delta E_i^{(Q)}\propto 3M^2-J(J+1). \tag{11}$$

The influence of the interface-induced energy level shifts on the internal atomic dynamics is described by the first term on the right-hand side of Eq. (8). The physical implications of this term become more transparent when distinguishing between the contributions of $\Delta H_A^{(S)}$ and $\Delta H_A^{(Q)}$. First, because $\Delta H_A^{(S)}$ produces a global shift of the energy levels, it modifies the atomic transition frequency in a Z-dependent way. As a result, the frequency detuning Δ between the laser and the atomic resonance, which plays an important role in the internal atomic dynamics, becomes space-dependent,

$$\Delta(Z)=\Delta_\infty+(\Delta E_g^{(S)}-\Delta E_e^{(S)})/\hbar, \tag{12}$$

where Δ_∞ denotes the free-space frequency detuning. Second, $\Delta H_A^{(Q)}$ lifts the degeneracy between the atomic Zeeman sublevels, provided, however, that the corresponding energy state has an angular momentum $J>1/2$ [see Eq. (11)]. In particular, $\Delta H_A^{(Q)}$ does not affect the ground state of alkali-metal atoms for which $J=1/2$ (this result still holds when taking into account the hyperfine structure of the atomic energy states). Moreover, in situations of practical interest, the influence of $\Delta H_A^{(Q)}$ on the frequency detuning Δ turns out to be almost always negligible compared to the contribution of $\Delta H_A^{(S)}$ or to the free-space frequency detuning. Finally, although we do not address the issue of external atomic dynamics in this paper, it is interesting to note that the interface-induced level shifts can manifest themselves in the atomic motion through a modification in the force experienced by the atomic center of mass (a point which is of great interest in the field of atom optics). This is because on the one hand, the radiative force arising from the laser field is modified through the Z-dependent frequency detuning Δ, and on the other hand, because the spatial variation of the energy levels leads to additional forces, such as van der Waals or Casimir forces.

C. Master equation treatment of spontaneous emission

We next consider the relaxation processes undergone by the atom as a result of its coupling with the vacuum quantum field. As is well known, these processes are conveniently described by a master equation for the atomic density matrix. In this section, we derive such an equation, taking into account the presence of the lower-lying dielectric medium. In particular, we show that the knowledge of the damping rates of two *classical* oscillating dipoles polarized parallel and orthogonal to the $z=0$ plane is sufficient to completely characterize the atomic relaxation associated with spontaneous emission.

1. Atom–quantum-field coupling

As stated above, the coupling between the atom and the quantized electromagnetic field (which is responsible for spontaneous emission) is described by the Hamiltonian

$V_{AR}=-\mathbf{D}\cdot\mathbf{E}$. The atomic dipole operator $\mathbf{D}$ changes sign under parity, and therefore has only zero matrix elements inside the Zeeman degeneracy subspaces of both the ground and excited states. Furthermore, because $|g\rangle$ and $|e\rangle$ have well-defined angular momenta, it is possible following the Wigner-Eckart theorem to write $\mathbf{D}$ in terms of a dimensionless, reduced dipole operator $\mathbf{d}$,

$$\mathbf{D}=\mathscr{D}\cdot\mathbf{d}, \tag{13}$$

whose matrix elements contain the Clebsch-Gordan coefficients associated with the addition of the angular momenta $1+J_g\rightarrow J_e$. In Eq. (13), $\mathscr{D}$ is a real number characterizing the electric dipole moment amplitude of the atomic transition. Denoting by P_g and P_e the projection operators on the ground and excited states, respectively, we decompose the reduced dipole operator as

$$\mathbf{d}=P_e\mathbf{d}P_g+P_g\mathbf{d}P_e=\mathbf{d}^+ +\mathbf{d}^- \tag{14}$$

and we expand $\mathbf{d}^+$ and $\mathbf{d}^-=(\mathbf{d}^+)^\dagger$ onto the standard basis $\{\mathbf{u}_{\pm1}=\mp(\mathbf{e}_x\pm i\mathbf{e}_y)/\sqrt{2},\mathbf{u}_0=\mathbf{e}_z\}$ (where $\mathbf{e}_{x,y,z}$ are the unitary vectors associated with the Cartesian coordinate system),

$$d_q^+=\mathbf{d}^+\cdot\mathbf{u}_q=(d_q^-)^\dagger. \tag{15}$$

The matrix elements of d_q^+ are then given by the simple expression

$$\left\langle J_eM_e\left|d_q^+|J_gM_g\right\rangle=\langle J_g\ 1M_gq|J_eM_e\right\rangle, \tag{16}$$

where $\langle J_g\ 1M_gq|J_eM_e\rangle$ is the Clebsch-Gordan coefficient connecting the Zeeman sublevels $|J_gM_g\rangle$ and $|J_eM_e=M_g+q\rangle$. Finally, using the rotating-wave approximation, the interaction Hamiltonian V_{AR} takes the more explicit form

$$V_{AR}=-\mathscr{D}\sum_{q=-1}^{1} d_q^+E_q^+ +d_q^-E_q^-\,, \tag{17}$$

where

$$\mathbf{E}^+=\sum_{q=-1}^{1} E_q^+\mathbf{u}_q=(\mathbf{E}^-)^\dagger \tag{18}$$

is the positive-frequency component of the electric field operator.

2. Relaxation equation for an arbitrary atomic observable

We now consider the effect of the atom-field coupling (17) on the time evolution of an arbitrary internal atomic observable S. Since we are not interested in the free evolution of the system, we turn to the interaction representation associated with the individual Hamiltonians of the atom and the field. It is well known that the relaxation processes undergone by the atom are then determined by the correlation functions of the electric field at the position of the atom

$$C_{qq'}^{\sigma\sigma'}[\omega]=\int d\tau e^{i\omega\tau}\langle E_q^\sigma(t+\tau)E_{q'}^{\sigma'}(t)\rangle, \tag{19}$$

where $\langle\ \rangle$ denotes the average in the vacuum state of the electromagnetic field, $\sigma,\sigma'=\pm$, and $q,q'=0,\pm1$. In our case, the correlation functions (19) can be expressed in terms of a small number of independent parameters. First, the positive-frequency component of the electric field operator only involves photon annihilation operators. Second, in the case we are studying here, the system is invariant under rotations about the z axis, leading to further simplifications. As a result, one gets

$$C_{qq'}^{\sigma\sigma'}[\omega]=C_q[\omega]\delta_{q,q'}\delta_{\sigma,+}\delta_{\sigma',-} \tag{20}$$

and

$$C_{-1}=C_1\equiv C_\parallel,\qquad C_0\equiv C_\perp\,. \tag{21}$$

Note that contrary to the free-space situation, where $C_{-1}=C_0=C_1$, the fluctuation spectrum of the vacuum is determined here by two different quantities $C_\parallel$ and $C_\perp$. This is a consequence of the vacuum isotropy breaking induced by the presence of the semi-infinite dielectric medium. Assuming a white noise fluctuation spectrum for the vacuum field, or more precisely a spectrum whose variations around the atomic resonance frequency are negligible, it is then possible using the Markov approximation to derive the relaxation equation for the expectation value $\langle S\rangle=\mathrm{tr}[\rho S]$ of any atomic observable S [9],

$$\left.\frac{d\langle S\rangle}{dt}\right|_{relax}=-\frac{\mathscr{D}^2}{2\hbar^2}\sum_q C_q[\omega_A]\langle d_q^+d_q^-S+Sd_q^+d_q^- -2\,d_q^+Sd_q^-\rangle, \tag{22}$$

where ω_A is the free-space atomic resonance frequency. Equations (16) and (22) indicate that for a given atomic transition, the relaxation equation of any atomic observable is completely characterized by the component of the vacuum fluctuation spectrum at the atomic transition frequency [10].

As is well known, the derivation of the functions $C_q[\omega_A]$ can be carried out from the radiation reaction viewpoint which only involves *classical* electrodynamics [11]. The somewhat surprising fact that quantities such as $C_q[\omega_A]$, which are quantum in nature, can be rigorously derived in the framework of classical theory can be understood as follows. First, the relaxation of the atomic dipole involves the vacuum fluctuation spectrum only at the atomic resonance frequency ω_A, irrespective of any other atomic energy states. In fact, the *same* coefficients $C_q[\omega_A]$ intervene in the relaxation of any quantum dipole of oscillation frequency ω_A. Specifically, this is the case for the relaxation of a quantum harmonic oscillator of oscillation frequency ω_A. Second, it is known that in the case of a harmonic oscillator linearly coupled to a harmonic reservoir, the evolution equation for the average value of the dipole operator is *identical* to that of the corresponding classical system [9]. It is therefore possible to connect the quantities $C_q[\omega_A]$ to the damping rates of properly chosen *classical* oscillating dipoles, which can be calculated in the framework of classical electrodynamics. This argument is made more rigorous and quantitative in Appendix A, where it is shown that

$$C_q[\omega_A]=\frac{\hbar^2}{\mathscr{D}^2}\Gamma_q. \tag{23}$$

In Eq. (23), Γ_q is the damping rate of a classical dipole with polarization $\mathbf{u}_q$, mass m, charge e, and oscillation frequency ω_A, these parameters being related to the atomic dipole matrix element $\mathscr{D}$ by

$$\frac{e^2}{m}=\frac{2\omega_A}{\hbar}\mathscr{D}^2. \tag{24}$$

Finally, combining Eqs. (22) and (23), one finds that the quantum relaxation equation of an arbitrary atomic observable S can be expressed rigorously in terms of the classical damping rates Γ_q,

$$\left.\frac{d\langle S\rangle}{dt}\right|_{relax}=-\sum_q\frac{\Gamma_q}{2}\langle d_q^+d_q^-S+Sd_q^+d_q^--2\,d_q^+Sd_q^-\rangle. \tag{25}$$

It is important to note that this technique for deriving the quantum relaxation equation of an atomic observable from the damping rate of classical oscillating dipoles is general and holds for other situations than the one considered in this paper (different geometry of the problem or different state of the electromagnetic field).

3. Relaxation equation for the atomic density matrix

The total contribution $\dot\rho_{relax}=\dot\rho_{relax,\infty}+\dot\rho_{relax,int}$ of spontaneous emission to the time evolution of the atomic density matrix can be readily derived from the preceding results. Considering two arbitrary Zeeman sublevels of the ground or the excited state of the atom, α and β, the matrix element $\langle\alpha|\dot\rho_{relax}|\beta\rangle$ follows straightforwardly from Eq. (25) with the particular choice $S_{\alpha\beta}=|\beta\rangle\langle\alpha|$. Distinguishing between the four blocks $\rho_{ab}=P_a\rho P_b$ (with $a,b=e,g$) of the atomic density matrix

$$\rho=\begin{pmatrix}\rho_{gg} & \rho_{ge}\\ \rho_{eg} & \rho_{ee}\end{pmatrix}, \tag{26}$$

one obtains the master equation associated with spontaneous emission

$$\left.\frac{d\rho_{ee}}{dt}\right|_{relax}=-\sum_{q=-1}^{1}\frac{\Gamma_q}{2}\{d_q^+d_q^-,\rho_{ee}\}, \tag{27a}$$

$$\left.\frac{d\rho_{eg}}{dt}\right|_{relax}=-\sum_{q=-1}^{1}\frac{\Gamma_q}{2}(d_q^+d_q^-)\rho_{eg}, \tag{27b}$$

$$\left.\frac{d\rho_{gg}}{dt}\right|_{relax}=\sum_{q=-1}^{1}\Gamma_q d_q^-\rho_{ee}d_q^+, \tag{27c}$$

where $\{A,B\}=AB+BA$ denotes the anticommutator between operators A and B, and where the equation for ρ_{ge} follows from Eq. (27b) and the relation $\rho_{ge}=(\rho_{eg})^\dagger$. It is important to note that the simple form of Eqs. (27) is associated with the particular choice of z as the direction *orthogonal* to the vacuum-dielectric interface, and with the corresponding definition of the standard basis $\mathbf{u}_q$. Furthermore, as expected, in the limiting case $z\to\infty$ where the atom is infinitely far from the interface, the rates Γ_q reduce to their common free-space value Γ_∞, and Eqs. (27) transform into their usual free-space expressions [7],

$$\left.\frac{d\rho_{ee}}{dt}\right|_{relax}\to\left.\frac{d\rho_{ee}}{dt}\right|_{relax,\infty}=-\Gamma_\infty\rho_{ee}, \tag{28a}$$

$$\left.\frac{d\rho_{eg}}{dt}\right|_{relax}\to\left.\frac{d\rho_{eg}}{dt}\right|_{relax,\infty}=-\frac{\Gamma_\infty}{2}\rho_{eg}, \tag{28b}$$

$$\left.\frac{d\rho_{gg}}{dt}\right|_{relax}\to\left.\frac{d\rho_{gg}}{dt}\right|_{relax,\infty}=\Gamma_\infty\sum_{q=-1}^{1}d_q^-\rho_{ee}d_q^+ \tag{28c}$$

(making use of the relation $\Sigma_{q=-1}^{1}d_q^+d_q^-=P_e$).

The physical interpretation of Eqs. (27) is particularly simple when working in the eigenbasis of M (z basis). The excited state operators $d_q^+d_q^-$ are purely diagonal in this basis [see Eq. (16)], with matrix elements equal to the square of the Clebsch-Gordan coefficients characterizing the coupling of the excited state Zeeman sublevels with a $\mathbf{u}_q$-polarized light. Consequently, as shown in Eq. (27a), the time evolution of the population of the excited state sublevel $|J_eM_e\rangle$ due to spontaneous emission corresponds to a pure damping process characterized by the relaxation rate

$$\Gamma_{J_e,M_e}=\sum_{q=-1}^{1}\Gamma_q\left\langle J_g\ 1M_gq\ \middle|\ J_eM_e\right\rangle^2. \tag{29}$$

A similar result is found for the Zeeman coherences between two excited state sublevels [Eq. (27a)] and for optical coherences between an excited state and a ground state Zeeman sublevel [Eq. (27b)], with a damping rate equal to the average of the relaxation rates of the corresponding populations. The presence of three terms in Eq. (29) reflects the fact that the excited state Zeeman sublevels can decay towards the ground state via three channels. These channels are associated with spontaneous emission of a $\mathbf{u}_q$-polarized photon and are characterized by a rate equal to the product of Γ_q and the square of the Clebsch-Gordan coefficient of the corresponding transition (see Fig. 2). It is important to note that contrary to the free-space situation, the lifetime of the different excited state Zeeman sublevels are different here, as a result of relaxation rates Γ_q. Finally, Eq. (27c) describes the feeding of the ground state Zeeman sublevels by the excited state as a result of spontaneous emission.

One might conclude from the preceding discussion that Eqs. (27) behave much the same as in free space, except for the differences in the lifetimes of the excited state Zeeman sublevels. Such a conclusion is *not* correct. In particular, the fact that Eqs. (27) only couple populations to populations and coherences to coherences holds in the z basis only. For example, working in the y basis, one can readily show that the *populations* of the excited state sublevels appear as feeding terms for some Zeeman *coherences* of the ground state (a property related to the isotropy breaking of the vacuum induced by the dielectric medium). One thus finds that the presence of the vacuum-dielectric interface modifies the atomic internal dynamics in both a quantitative and a qualitative way as compared to the case of an atom in free space. It is important to emphasize that such a result is characteris-

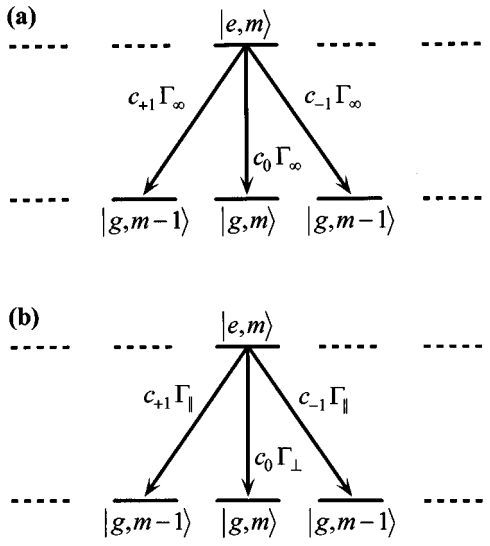

FIG. 2. Radiative damping of the excited-state populations. The excited-state Zeeman sublevel $|e,m\rangle$ can decay towards the ground state via three channels. These channels are associated with spontaneous emission of a $\mathbf{u}_{q=0,\pm1}$-polarized photon and are characterized by a rate equal to the product of Γ_q and the square c_q of the Clebsch-Gordan coefficient corresponding to the transition. (a) In free space, $\Gamma_{q=0,\pm1}=\Gamma_\infty$, hence all the excited-state sublevels have the same lifetime. (b) In the presence of a vacuum-dielectric interface, $\Gamma_{q=\pm1}\neq\Gamma_{q=0}$, hence the sublevels have different lifetimes.

tic of a *multilevel* atom. In the case of a two-level system, the interface indeed reduces to a simple quantitative modification of the excited state lifetime, so that no qualitatively different physical phenomena are expected.

D. Optical Bloch equations

The optical Bloch equations describing the internal dynamics of an atom interacting with laser light in the vicinity of a vacuum-dielectric interface are readily obtained in the Markov approximation by adding the above-described contributions of the reservoir to those of the laser field. Returning to the Schrödinger picture and using the rotating wave approximation, this yields

$$\dot{\rho}_{ee}=-\sum_{q=-1}^{1}\frac{\Gamma_q}{2}\{d_q^+d_q^-,\rho_{ee}\}+\frac{1}{i\hbar}[\Delta H_e,\rho_{ee}]-\frac{1}{i\hbar}[\mathbf{D}^+\cdot\mathscr{E}_L^+\tilde{\rho}_{ge}-\tilde{\rho}_{eg}\mathbf{D}^-\cdot\mathscr{E}_L^-], \tag{30a}$$

$$\dot{\tilde{\rho}}^{eg}=-\sum_{q=-1}^{1}\frac{\Gamma_q}{2}(d_q^+d_q^-)\tilde{\rho}_{eg}+i\left(\Delta_\infty+\frac{\Delta H_g-\Delta H_e}{\hbar}\right)\tilde{\rho}_{eg}-\frac{1}{i\hbar}[\mathbf{D}^+\cdot\mathscr{E}_L^+\rho_{gg}-\rho_{ee}\mathbf{D}^+\cdot\mathscr{E}_L^+], \tag{30b}$$

$$\dot{\rho}_{gg}=\sum_{q=-1}^{1}\Gamma_q d_q^-\rho_{ee}d_q^++\frac{1}{i\hbar}[\Delta H_g,\rho_{gg}]-\frac{1}{i\hbar}[\mathbf{D}^-\cdot\mathscr{E}_L^-\tilde{\rho}_{eg}-\tilde{\rho}_{ge}\mathbf{D}^+\cdot\mathscr{E}_L^+], \tag{30c}$$

where

$$\Delta H_b=P_b\Delta H_A P_b\quad(b=e,g) \tag{31}$$

denote the effective Hamiltonians associated with the interface-induced energy level shifts, $\mathscr{E}_L^+$ ($\mathscr{E}_L^-$) is the positive (negative) frequency part of the monochromatic laser electric field

$$\mathscr{E}_L(t)=\mathscr{E}_L^+\exp(-i\omega_L t)+\mathscr{E}_L^-\exp(i\omega_L t), \tag{32}$$

and where

$$\tilde{\rho}_{eg}=\rho_{eg}e^{i\omega_L t}=\tilde{\rho}_{ge}^\dagger \tag{33}$$

is the expression of the optical coherences in the so-called rotating frame. Note that in most experimental situations, it is a good approximation to replace the second term on the right-hand side of Eq. (30b) with the simpler one $i\Delta(Z)\tilde{\rho}_{eg}$ (see Sec. II B).

III. QUANTITATIVE DERIVATION OF ENERGY SHIFTS, SPONTANEOUS EMISSION RATES, AND RADIATION DIAGRAMS

As shown in the preceding section, the internal dynamics of a multilevel atom interacting with a quasiresonant laser field in the vicinity of a vacuum-dielectric interface are entirely determined, on the one hand, by the atomic level shifts, and, on the other hand, by the damping rates of a classical oscillating dipole polarized parallel or orthogonal to the interface. Several techniques for evaluating these parameters can be found in existing literature; however, they are occasionally impractical for given experimental geometries, or inadequate for the case of multilevel atoms. This section presents guidelines particularly adapted to the situation of alkali atoms located close to a single dielectric medium [Fig. 3(a)] or a dielectric waveguide [Fig. 3(b)], both of which are of current experimental interest [1,5].

A. London–van der Waals energy shifts

The calculation of energy level shifts at a vacuum-dielectric interface has been considered by several authors (see, for example, [13,14] and references therein). In this section, we restrict ourselves to the energy shifts in the immediate vicinity of the interface ($Z<\lambda_A=c/\omega_A$), where they take their largest values. In this region, the level shifts arise essentially from the London–van der Waals interaction, hence (see Sec. II)

$$\Delta H_A\approx\Delta H_{es}. \tag{34}$$

The effective Hamiltonian associated with the level shifts can thus be derived in the framework of *electrostatics* theory using the method of images for dielectrics [15]. In this approach, the component of the electric field of the atomic dipole $D_\parallel$ ($D_\perp$) reflected by the dielectric medium back onto the location of the atom appears to arise from an ensemble of one or more effective dipoles $D_{\parallel,n}=d_{\parallel,n}D_\parallel$ ($D_{\perp,n}=-d_{\perp,n}D_\perp$) located at positions z_n. Combining these, one obtains [16]

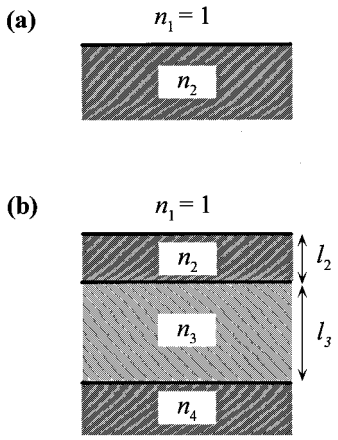

FIG. 3. Experimental geometries considered for the quantitative derivation of energy shifts, spontaneous emission rates, and radiation patterns. (a) A single interface separates the vacuum (medium 1) and a semi-infinite dielectric medium 2 of refractive index n_2. (b) A dielectric waveguide consisting of two dielectric layers 2 and 3 of thicknesses l_2 and l_3, respectively, is deposited on a semi-infinite dielectric medium 4.

$$\Delta H_{es} = \frac{1}{8\pi\epsilon_0} \sum_n \frac{D_\parallel^2 d_{\parallel,n} + 2D_\perp^2 d_{\perp,n}}{|Z - z_n|^3}. \tag{35}$$

We now evaluate the coefficients $d_{\parallel,n}$ and $d_{\perp,n}$ and the London–van der Waals Hamiltonian ΔH_{es} for the two experimental geometries of Fig. 3.

1. Single dielectric medium

In the geometry of Fig. 3(a), there is a single homogeneous dielectric medium in the region $z<0$, and the reflected electric field is correspondingly described by a single effective dipole located at position $-Z$, of amplitude [17]

$$d_\parallel = d_\perp = \frac{1-\epsilon_2}{1+\epsilon_2}, \tag{36}$$

where ϵ_2 is the dielectric constant of medium 2. This yields the well-known van der Waals interaction Hamiltonian

$$\Delta H_{es} = -\frac{\epsilon_2 - 1}{\epsilon_2 + 1} \frac{1}{64\pi\epsilon_0} \frac{D_\parallel^2 + 2D_\perp^2}{Z^3}. \tag{37}$$

2. Dielectric waveguide

The geometry of Fig. 3(b) is more complicated because the atomic dipole electric field is multiply reflected by the different interfaces of the multilayered dielectric medium. To remain consistent with our electrostatic assumption, we neglect the contribution of multiply reflected fields propagating over distances significantly larger than $\lambda\!\!\!^{-}_A$. In the case of the dielectric waveguides used in atom optics [5], the thickness l_2 of the dielectric layer 2 is a small fraction of the optical wavelength $\lambda_A = 2\pi\lambda\!\!\!^{-}_A$ whereas that of layer 3, l_3, is of order λ_A. We therefore neglect reflections at the interface between media 3 and 4 [see Fig. 3(b)], or equivalently set $\epsilon_4 = \epsilon_3$. It is then straightforward to show that the field at the location of the atomic dipole resulting from multiple reflections inside medium 2 is described by the following infinite ensemble of image dipoles:

$$d_0 = \alpha_{12}, \tag{38a}$$

$$z_0 = -Z, \tag{38b}$$

$$d_{n\geq 1} = \frac{1-\alpha_{21}^2}{\alpha_{21}} (\alpha_{21}\alpha_{23})^n, \tag{39a}$$

$$z_{n\geq 1} = -Z - 2nl_2, \tag{39b}$$

where

$$\alpha_{ij} = \frac{\epsilon_i - \epsilon_j}{\epsilon_i + \epsilon_j}. \tag{40}$$

These expressions apply to both $d_{\parallel,n}$ and $d_{\perp,n}$. Combining Eqs. (38) and (39) with (35) yields the expression of the Hamiltonian describing the London–van der Waals interaction between the atom and the dielectric waveguide

$$\Delta H_{es} = -\frac{D_\parallel^2 + 2D_\perp^2}{64\pi\epsilon_0} \left(\frac{\alpha_{21}}{Z^3} + \frac{\alpha_{21}^2 - 1}{\alpha_{21}} \sum_{n=1}^{\infty} \frac{(\alpha_{21}\alpha_{23})^n}{(Z + nl_2)^3} \right). \tag{41}$$

The first term inside the parentheses is analogous to expression (37) and corresponds to the London–van der Waals interaction between the atomic dipole and medium 2 alone. This is the leading contribution as Z approaches zero. The second term in Eq. (41) stems from the presence of the interface between media 2 and 3. We note that in practical situations the generic term of the sum is a rapidly decreasing function of n, so that in effect the infinite sum reduces to a small number of terms, and the electrostatic assumption remains legitimate. In the situation of interest in atom optics [5], where $\epsilon_2 > \epsilon_3$ and $\epsilon_2 > \epsilon_1$, the second term in Eq. (41) represents a nonalternating series summation which can become quite significant. This is because in this event, medium 2 confines the dipole field and serves as an effective waveguide, resulting in a field enhancement near its interfaces. Another limiting case of interest is that of a vanishing dielectric waveguide, or more generally $l_2/Z \to 0$. In this case, Eq. (41) takes the simple form

$$\Delta H_{es} \approx -\frac{D_\parallel^2 + 2D_\perp^2}{64\pi\epsilon_0} \left(\frac{\alpha_{31}}{Z^3} + \frac{3\,l_2}{Z^4} \frac{\alpha_{23}(1-\alpha_{21}^2)}{(1-\alpha_{21}\alpha_{23})^2} \right), \tag{42}$$

whose leading term now corresponds to the interaction potential between the atomic dipole and medium 3 alone, as expected physically.

TABLE I. Values of the effective principal quantum number n^* for the ground state and first excited states of sodium, rubidium, and cesium (after Ref. [18]).

	s	*p*
Na	1.627	2.117
Rb	1.805	2.293
Cs	1.869	2.362

3. Matrix elements of the London–van der Waals interaction potential

(a) General. As is manifest in Eqs. (37) and (41), the van der Waals energy shifts are determined, on the one hand, by experimental parameters (refractive indices, thickness of the dielectric layers), and, on the other hand, by the purely internal operator

$$W = D_{\parallel}^2 + 2D_{\perp}^2 = e^2(x_e^2 + y_e^2 + 2z_e^2), \tag{43}$$

where e is the electron charge and x_e, y_e, z_e are the Cartesian coordinates of the electron in the atomic center-of-mass frame. In order to calculate the matrix elements of the operator W we distinguish, following the symmetry arguments of Sec. II B, between the scalar part $W^{(S)}$ and the quadrupolar part $W^{(Q)}$ of W

$$W = W^{(S)} + W^{(Q)} = e^2\left(\frac{4}{3}r_e^2 + \frac{1}{3}r_e^2 Q\right), \tag{44}$$

where

$$Q = \sqrt{\frac{16\pi}{5}}Y_{20}(\theta,\phi) \tag{45}$$

is independent of the electron-atomic nucleus distance $r_e = \sqrt{x_e^2 + y_e^2 + z_e^2}$. The London–van der Waals energy level shifts are thus entirely determined by the matrix elements of the operators r_e^2 and Q.

(b) Fine structure. Let us first consider the fine structure of alkali atoms. In most cases of experimental interest, the van der Waals energy shifts are much smaller than the fine splitting between the atomic energy levels $|i\rangle = |n,l,J,M\rangle$, and can therefore be calculated using first order perturbation theory. One thus has

$$\Delta E_i \propto \langle n,l,J,M|W|n,l,J,M\rangle \tag{46}$$

and the energy level shifts can be readily evaluated by combining Eq. (44) and the relations [8]

$$\langle n,l,J,M|r_e^2|n,l,J,M\rangle = \langle n,l|r_e^2|n,l\rangle \approx a_0^2 n_i^{*2}\frac{5n_i^{*2} + 1 - 3l(l+1)}{2}, \tag{47}$$

$$\langle n,l,J,M|Q|n,l,J,M\rangle = (-1)^{M+1/2}2(2J+1) \times \begin{pmatrix} J & J & 2 \\ 1/2 & -1/2 & 0 \end{pmatrix}_{3j} \times \begin{pmatrix} J & J & 2 \\ -M & M & 0 \end{pmatrix}_{3j}, \tag{48}$$

where a_0 is the Bohr radius, n_i^* denotes the effective principal quantum number of the atomic level $|i\rangle$, and $(\cdots)_{3j}$ is a $3j$ Wigner coefficient. The values of n_i^* associated with the ground state and first excited states of alkali atoms are well known and provide accurate estimates of $\langle i|r_e^2|i\rangle$ through Eq. (47) [18]. They are given in Table I for the ground state (s) and the first excited state (p) of sodium, rubidium, and cesium.

(c) Hyperfine structure. Let us now consider the hyperfine structure of the alkali energy spectra. When the atom-dielectric distance is sufficiently large that the London–van der Waals energy shifts are small compared to the hyperfine splitting of the atomic levels, then the energy shifts can again be calculated using first order perturbation theory, as above. However, when the atom gets closer to the vacuum-dielectric interface, the London–van der Waals energy shifts eventually become comparable to or even larger than the hyperfine splitting, so that a coupling between the hyperfine sublevels of a same magnetic quantum number m can take place through the quadrupolar part of the London–van der Waals coupling. In such a case, it becomes necessary to diagonalize the restriction of operator Q to the corresponding hyperfine subspace. Both situations can be treated straightforwardly using the relations [8,19]

$$\langle n,l,J,I,F,M|r_e^2|n,l,J,I,F,M\rangle = \langle n,l|r_e^2|n,l\rangle \approx a_0^2 n_i^{*2}\frac{5n_i^{*2} + 1 - 3l(l+1)}{2}, \tag{49}$$

$$\langle n,l,J,I,F,M|Q|n,l,J,I,F',M\rangle = (-1)^{2J+I-M-1/2}2(2J+1)\sqrt{(2F+1)(2F'+1)} \times \begin{pmatrix} J & J & 2 \\ 1/2 & -1/2 & 0 \end{pmatrix}_{3j} \begin{Bmatrix} F & F' & 2 \\ J & J & I \end{Bmatrix}_{6j} \begin{pmatrix} F & F' & 2 \\ -M & M & 0 \end{pmatrix}_{3j}, \tag{50}$$

where I denotes the nuclear spin of the atom, and $\{\ \}_{6j}$ is a $6j$ Wigner coefficient.

B. Dipole damping rates and radiation patterns

The damping rates of classical oscillating dipoles located in the vicinity of a dielectric medium have been calculated and discussed for many years [20–22]. In addition, the dipole radiation patterns, which are also experimentally measurable, have been derived in the case of a single dielectric interface [22]. In this section, we present a simple and powerful method for deriving these quantities in more general situations. The method is based on Lorentz's reciprocity theorem [23], and allows one to simultaneously calculate the radiation patterns and the damping rates of classical dipoles.

It applies in the same straightforward way to the case of a single or a multilayered dielectric medium, and to the case of lossless or absorbing media. For the sake of clarity of presentation, we first describe the principle of the method (Sec. III B 1) and defer its derivation to Appendix B. The method is applied to the case of a single dielectric medium, where it is shown to yield the same results as in [22] (Sec. III B 2), and also to the case of a dielectric waveguide for which the dipole radiation patterns and damping rates are obtained for the first time (Sec. III B 3).

1. Principle of the method

We consider the angular distribution of the radiation emitted by a classical oscillating dipole located in vacuum a distance Z above a single or multilayered dielectric medium (see Fig. 1), and polarized either parallel ($\parallel$) or perpendicular ($\perp$) to the vacuum-dielectric interface. We look for analytical expressions for the normalized (time-averaged) power $P_{\parallel,\perp}(\theta,\varphi)$ radiated into the direction (θ,φ) in the differential solid angle $d\Omega=\sin\theta d\theta d\varphi$, where θ and φ are the canonical spherical coordinates. The normalization is chosen so that the integration of $P_{\parallel,\perp}(\theta,\varphi)$ over all space gives

$$\int P_{\parallel,\perp}(\theta,\varphi)d\Omega=\Gamma_{\parallel,\perp}(Z)/\Gamma_{\infty}, \tag{51}$$

where $\Gamma_{\parallel,\perp}(Z)$ and Γ_{∞} are the damping rates with and without an interface, as defined in Sec. II C and Appendix A. In the geometries considered in this paper, the derivation of the radiation patterns $P_{\parallel,\perp}(\theta,\varphi)$ involves the calculation of three quantities that are independent of the azimuthal angle φ. First, in the case of a $\perp$-polarized dipole the radiation consists only of plane waves polarized parallel to their propagation planes (p or TM waves), and the radiation pattern is independent of φ because of azimuthal symmetry; hence

$$P_{\perp}(\theta,\varphi)\equiv\mathscr{P}_{\perp}^{p}(\theta). \tag{52}$$

Second, in the case of a $\parallel$-polarized dipole, we define $\varphi=0$ as the dipole polarization direction, and the radiation pattern takes the form

$$P_{\parallel}(\theta,\varphi)=\cos^2\varphi\mathscr{P}_{\parallel}^{p}(\theta)+\sin^2\varphi\mathscr{P}_{\parallel}^{s}(\theta), \tag{53}$$

where $\mathscr{P}_{\parallel}^{p}(\theta)$ denotes the radiation distribution of the wave components that are p-polarized, and where $\mathscr{P}_{\parallel}^{s}(\theta)$ denotes the radiation distribution of the wave components that are polarized perpendicular to their propagation planes (s or TE waves). In other words, $\mathscr{P}_{\parallel}^{p}(\theta)$ is the distribution of the total radiation emitted in the $\varphi=0$ plane, and $\mathscr{P}_{\parallel}^{s}(\theta)$ is the distribution of the total radiation emitted in the $\varphi=\pi/2$ plane.

The basic principle of the method for deriving the radiation patterns ($\mathscr{P}_{\perp}^{p}$, $\mathscr{P}_{\parallel}^{p}$, and $\mathscr{P}_{\parallel}^{s}$) is that the outgoing power emitted by the dipole in the direction (θ,φ) can be calculated by considering an incoming wave propagating from infinity in the opposite direction $(\pi-\theta,\varphi+\pi)$. In general, and depending on its direction of origin, this incoming wave can undergo multiple reflections and/or transmissions at the various dielectric interfaces it encounters before it is incident on the dipole. We separately consider incoming p-polarized waves, of amplitude $\mathscr{E}_{in}^{p}$, and incoming s-polarized waves of amplitude $\mathscr{E}_{in}^{s}$. These result in p and s polarized electric fields at the dipole location, $\mathscr{E}_{dip}^{p}$ and $\mathscr{E}_{dip}^{s}$, respectively. We denote by $\mathscr{E}_{\parallel}^{p,s}$ and $\mathscr{E}_{\perp}^{p,s}$ the projections of $\mathscr{E}_{dip}^{p,s}$ onto the directions parallel and perpendicular to the interface ($\mathscr{E}_{\perp}^{s}$ is, of course, zero). We further define the "coupling" efficiencies between incoming and incident fields as

$$L_{\parallel,\perp}^{p}(\theta)=\left|\frac{\mathscr{E}_{\parallel,\perp}^{p}(Z)}{\mathscr{E}_{in}^{p}}\right|^2 \tag{54a}$$

and

$$L_{\parallel}^{s}(\theta)=\left|\frac{\mathscr{E}_{\parallel}^{s}(Z)}{\mathscr{E}_{in}^{s}}\right|^2. \tag{54b}$$

Then, according to the Lorentz reciprocity theorem (derived in Appendix B), the outgoing power of a radiating dipole can be directly calculated from the incoming "coupling" efficiencies through the simple relations

$$\mathscr{P}_{\parallel,\perp}^{s,p}(\theta)=\frac{3}{8\pi}n(\theta)L_{\parallel,\perp}^{s,p}(\theta), \tag{55}$$

where $n(\theta)$ denotes the index of refraction of the outermost dielectric layer located in the direction θ [in particular, $n(\theta)=1$ for $0\leqslant\theta\leqslant\pi/2$].

It is important to note that this way of deriving dipole radiation patterns, and consequently dipole damping rates [see Eq. (51)], presents four important advantages. First, it relies on only elementary calculations because the derivation of the coefficients $L_{\parallel,\perp}^{s,p}(\theta)$ involves only Fresnel transmission and reflection coefficients at dielectric interfaces [24]. Second, it applies in exactly the same way for lossless and absorbing dielectric media (see Appendix B). Third, it provides a direct physical insight into the Z dependence of the dipole radiation patterns and damping rates because it intrinsically identifies the contributions of the different emission angles and of s and p waves. Fourth, the relation between dipole radiation and field coupling efficiency provides a very intuitive understanding of the radiation pattern characteristics. In particular, radiation by a dipole will predominantly occur in the output directions associated with strong coupling efficiencies for the corresponding incoming fields.

2. Case of a single dielectric medium

As a first illustration of the method, we consider the simple case of a dipole located above a single dielectric medium of refractive index n_2 [case of Fig. 3(a)]. As previously emphasized by Lukosz and Kunz [22], it is convenient to distinguish between three different regions in the dipole radiation patterns (Fig. 4). The first region (I), corresponding to radiation emission into the vacuum ($0\leqslant\theta\leqslant\pi/2$), is characterized for a given direction (θ,φ) by an interference between the plane wave directly emitted in the direction (θ,φ) and the reflected portion of the plane wave initially emitted in the direction $(\pi-\theta,\varphi)$. This interference, apparent in the expressions of $L_{\parallel,\perp}^{s,p}(\theta)$ [see Eqs. (C5 a), (C6a), and (C7a) is responsible for the oscillating behavior of the dipole

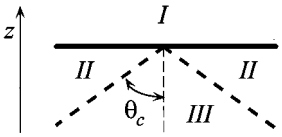

FIG. 4. Regions I, II, and III of the dipole radiation patterns corresponding to radiation into the vacuum (I), or into the lower-lying dielectric medium at angles larger (II) or smaller (III) than the critical angle θ_c.

damping rates as a function of Z (see Fig. 7). The second region (II) corresponds to radiation emission into the dielectric medium at angles exceeding the critical angle θ_c (defined by $\sin\theta_c = 1/n_2$). Radiation into this region ($\pi/2 \leqslant \theta \leqslant \pi - \theta_c$) originates from evanescent waves in the dipole's near field that are transformed by the interface into propagating plane waves in the dielectric medium. We note the exponential decay of this emission as a function of Z in expressions (C5b), (C6b), and (C7b). The dipole damping rates are usually dominated by this emission contribution for small Z. Finally, the third region (III) corresponds to radiation emission into the dielectric medium at angles smaller than the critical angle θ_c ($\pi - \theta_c \leqslant \theta \leqslant \pi$). It consists of propagating plane waves emitted by the dipole that are partially transmitted into the dielectric medium, and is independent of Z [see Eqs. (C5c), (C6c), and (C7c)].

The dipole radiation patterns derived from expression (55) and the coefficients $L_{\parallel,\perp}^{s,p}(\theta)$ of Appendix C are illustrated in Figs. 5 and 6 for $n_2 = 1.5$ and $Z = 0$ [Figs. 5(a,b) and 6(a)] and $Z = \lambda_A$ [Figs. 5(c,d) and 6(b)]. Note the sharp emission peak around the critical angle, and the rapid decay of region II of the radiation pattern as the dipole is removed from the vacuum-dielectric interface. The Z dependence of the dipole damping rates obtained from Eq. (51) is illustrated for the same parameters in Fig. 7, where qualitative differences in the contributions of the three regions of the radiation pattern are apparent. It is important to note that all our results are obtained directly from the coefficients $L_{\parallel,\perp}^{s,p}(\theta)$ and are strictly identical to those derived previously [20–22] using other techniques. In particular, an analytical expression for the dipole damping rates can be readily obtained by inspection of Eqs. (51), (C5), (C6), and (C7). Using elementary algebra, it can be expressed in the compact form [21]

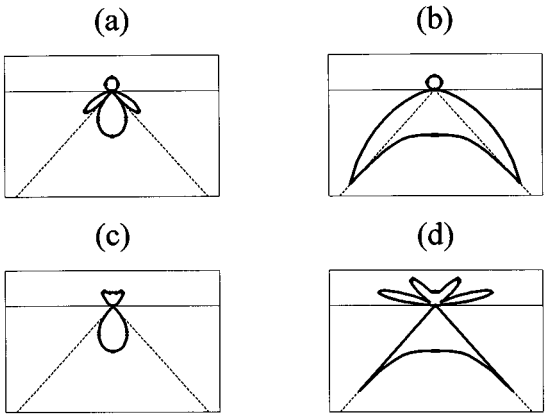

FIG. 5. Polar radiation pattern of a $\parallel$-polarized dipole located a distance Z above a single dielectric medium of refractive index $n_2 = 1.5$. (a) $\mathscr{P}_{\parallel}^{p}(Z=0)$. (b) $\mathscr{P}_{\parallel}^{s}(Z=0)$. (c) $\mathscr{P}_{\parallel}^{p}(Z=\lambda_A)$. (d) $\mathscr{P}_{\parallel}^{s}(Z=\lambda_A)$. All four diagrams have the same scale. The dashed line corresponds to the boundary between regions II and III of the radiation diagrams (i.e., the critical angle θ_c). Note the rapid decay of region II as the dipole is removed from the vacuum-dielectric interface.

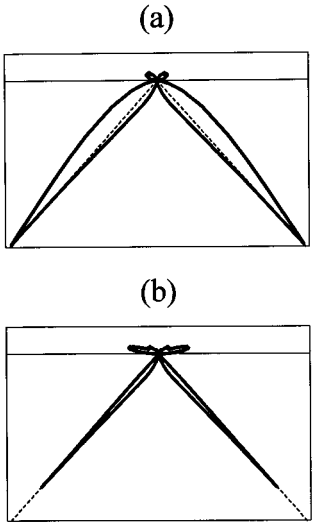

FIG. 6. Same as Fig. 5, but for a $\perp$-polarized dipole. (a) $\mathscr{P}_{\parallel}^{p}(Z=0)$. (b) $\mathscr{P}_{\parallel}^{p}(Z=\lambda_A)$.

$$\Gamma_{\perp}(Z) = \Gamma_{\infty}\left[1 + \frac{3}{2}\mathrm{Re}\int_0^{\infty} \frac{u^3 du}{\sqrt{1-u^2}}\rho^{p}(u)\exp(2ikZ\sqrt{1-u^2})\right], \tag{57}$$

$$\Gamma_{\parallel}(Z) = \Gamma_{\infty}\left[1 + \frac{3}{4}\mathrm{Re}\int_0^{\infty} \frac{u\,du}{\sqrt{1-u^2}} \times [\rho^{p}(u) + (u^2-1)\rho^{s}(u)]\exp(2ikZ\sqrt{1-u^2})\right], \tag{58}$$

with the appropriate Fresnel reflection coefficients for p and s waves

$$\rho^{p}(u) = \frac{n_2^2\sqrt{1-u^2} - \sqrt{n_2^2-u^2}}{n_2^2\sqrt{1-u^2} + \sqrt{n_2^2-u^2}}, \tag{59a}$$

$$\rho^{s}(u) = \frac{\sqrt{1-u^2} - \sqrt{n_2^2-u^2}}{\sqrt{1-u^2} + \sqrt{n_2^2-u^2}}. \tag{59b}$$

3. Case of a multilayered dielectric medium

We now consider the situation of Fig. 3(b) where the dipole is located above a dielectric waveguide. As in the preceding case, we distinguish between three regions of the dipole radiation pattern

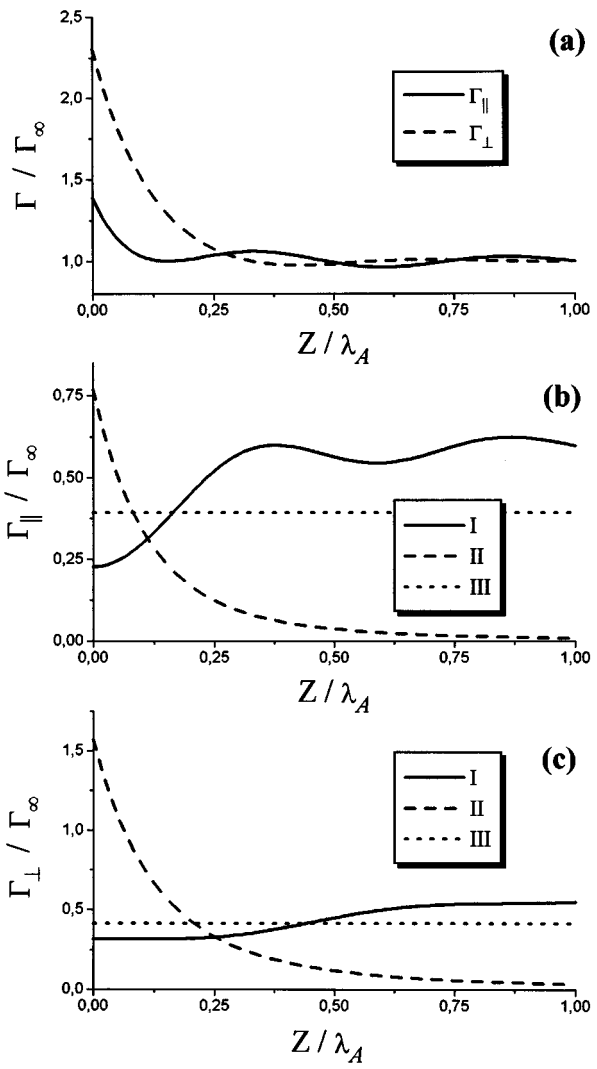

FIG. 7. Z dependence of the dipole damping rates in the experimental geometry of Fig. 3(a). Total damping rates $\Gamma_{\parallel,\perp}$ for $\parallel,\perp$-polarized dipoles (a) and respective contributions of regions I, II, and III to $\Gamma_\parallel$ (b) and $\Gamma_\perp$ (c).

$$(\mathrm{I}): \quad 0 \leqslant \theta \leqslant \pi/2, \tag{60a}$$

$$(\mathrm{II}): \quad \pi/2 \leqslant \theta \leqslant \pi - \theta_c\,, \tag{60b}$$

$$(\mathrm{III}): \quad \pi - \theta_c \leqslant \theta \leqslant \pi, \tag{60c}$$

where θ_c is the critical angle for total internal reflection at the vacuum-waveguide interface, now defined by

$$\sin\theta_c = 1/n_4\,. \tag{61}$$

Again, region I involves the far-field interference between plane waves directly emitted into the direction $(0 \leqslant \theta \leqslant \pi/2, \varphi)$ and indirectly emitted into this direction after reflection off the waveguide structure. The reflection coefficient in the latter case is given in Appendix D. Similarly, region II involves the transformation of evanescent waves in medium 1 into propagating waves in medium 4, and region III involves the transformation of propagating waves in medium 1 into propagating waves in medium 4. The pertinent

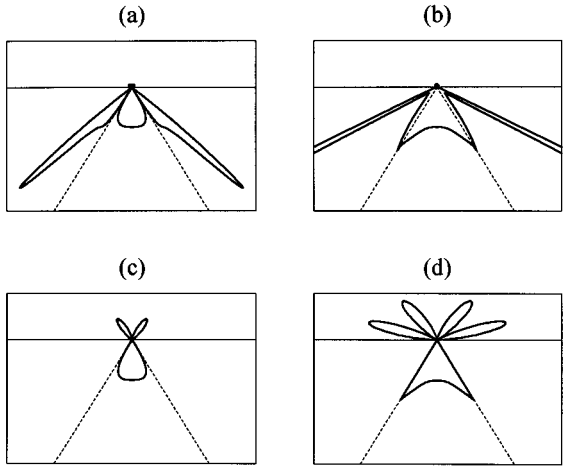

FIG. 8. Polar radiation pattern of a $\parallel$-polarized dipole located a distance Z above the dielectric waveguide of Ref. [5], corresponding to the parameters $n_2 = 2.37$, $l_2 = 87$ nm, $n_3 = 1.46$, $l_3 = 350$ nm, $n_4 = 1.894$, and $\lambda_A = 785.8$ nm. (a) $\mathscr{P}_\parallel^p(Z=0)$. (b) $\mathscr{P}_\parallel^s(Z=0)$. For the sake of presentation, the sharp emission peak around $\theta_{res} \approx 63°$ has been truncated. The peak size $\mathscr{P}_\parallel^s(\theta = \pi - \theta_{res})$ is actually about 40 times larger than the limit of the plot. (c) $\mathscr{P}_\parallel^p(Z=\lambda_A)$. (d) $\mathscr{P}_\parallel^s(Z=\lambda_A)$.

transmission coefficient for these transformations is also given in Appendix D. In contrast to the case of a single dielectric medium, this transmission coefficient can contain poles at specific ''resonance'' angles which are associated with waveguide modes [5]. An inspection of Eqs. (D2) reveals that these poles can only exist in region II, that is, they necessarily involve the coupling of the dipole radiation into medium 4 via evanescent waves. The poles correspond to resonances in the coupling efficiency (see Sec. III B 1), and as such, because of the relation between coupling efficiency and radiation, may have an important contribution to the dipole damping rate when the dipole is near the interface. This contribution decays exponentially as a function of the dipole position Z, as is characteristic of radiation in region II.

The features described above are clearly visible in Figs. 8–10, where we illustrate the dipole radiation patterns for $Z=0$ [Figs. 8(a,b) and 9(a)] and $Z=\lambda_A$ [Figs. 8(c,d) and 9(b)], and the Z dependence of the dipole damping rates, respectively. All three figures have been obtained using the method described in Sec. III B 1 by considering the waveguide parameters of Ref. [5] chosen to yield a high-Q waveguide factor for s-polarized waves having an incidence angle $\theta_{res} \approx 63°$. As a consequence, the contribution of region II in the radiation pattern and damping rate of the $\parallel$-polarized dipole becomes comparable to that of the $\perp$-polarized dipole, as shown in Figs. 8(a) (note the sharp emission peak around the resonance angle θ_{res}), 9(a), and 10(b,c). We have verified that this feature, which is never observed in the case of a single dielectric medium (see, for example, Fig. 7), actually arises from the contribution of waveguide modes.

IV. CONCLUSION

In conclusion, we have addressed the timely issue of the modification of internal atomic dynamics in the vicinity of

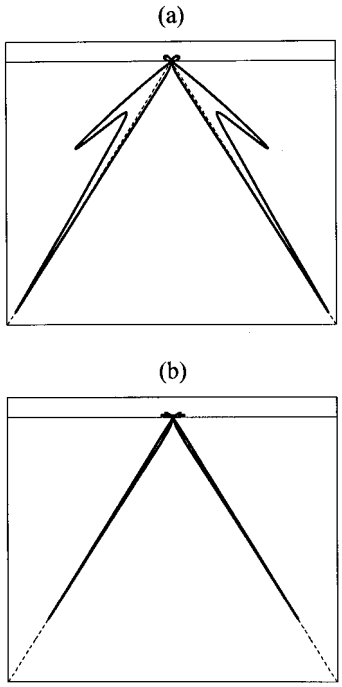

FIG. 9. Same as Fig. 8, but for a $\perp$-polarized dipole. (a) $\mathscr{P}_{\parallel}^{p}(Z=0)$. (b) $\mathscr{P}_{\parallel}^{p}(Z=\lambda_A)$. Note the absence of sharp emission peak due to the dielectric waveguide design and to the polarization of the dipole radiation.

the interface between a vacuum and a simple or multilayered dielectric medium. Optical Bloch equations have been derived, taking into account the modifications of spontaneous emission rates and energy levels experienced by the atom. In particular, these equations should occasion a more accurate description of van der Waals energy shifts as measured by reflection spectroscopy [1]. They should also prove useful in the emerging field of laser cooling and trapping inside cavities designed to modify spontaneous emission. Simple expressions for the van der Waals energy shifts of alkali atoms have been obtained, which should be of interest in atomic optics. Finally, a simple and powerful method for deriving spontaneous emission rates and radiation patterns (also of interest in atom optics) has been presented, which applies to both lossless and absorbing media. This method based on the Lorentz reciprocity theorem should prove useful generally.

ACKNOWLEDGMENTS

We are very grateful to A. Landragin and F. Nez for their most efficient and helpful contributions. We also acknowledge stimulating and clarifying discussions with A. Aspect, Y. Castin, J. Dalibard, D. Delande, M. Ducloy, C. Jurczak, R. Kaiser, H. Rigneault, N. Vansteenkiste, and C. Westbrook. J. C. M. is particularly grateful to W. W. Webb and J. Mlynek for financial support.

APPENDIX A: DERIVATION OF THE FORMULA (23)

Consider a quantum harmonic oscillator of mass m and charge e oscillating at the frequency ω_A. The dipole operator of such a system in the interaction representation reads

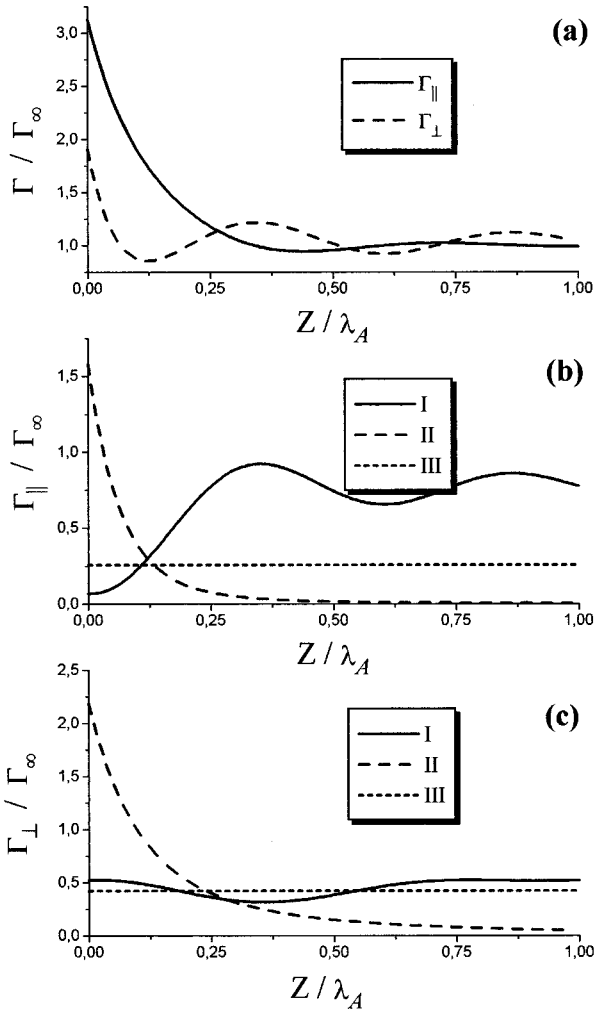

FIG. 10. Z dependence of the dipole damping rates in the case of Fig. 8. Total damping rates $\Gamma_{\parallel,\perp}$ for $\parallel,\perp$-polarized dipoles (a) and contributions of regions I, II, and III to $\Gamma_{\parallel}$ (b) and $\Gamma_{\perp}$ (c).

$$\mathbf{D}_{HO}=\mathscr{D}_{HO}\sum_{q=-1}^{1} a_q\mathbf{u}_q+a_q^{\dagger}\mathbf{u}_q^{*}, \tag{A1}$$

where a_q and $a_q^{\dagger}$ are the annihilation and creation operators associated with the excitation modes of the oscillator along the $\mathbf{u}_q$ direction, and where $\mathscr{D}_{HO}=e\sqrt{\hbar/2m\omega_A}$. As in the case of an atomic dipole (Sec. II C 2), the relaxation equation for any observable S_{HO} of the harmonic oscillator reads

$$\left.\frac{d\langle S_{HO}\rangle}{dt}\right|_{relax}=-\frac{\mathscr{D}_{HO}^2}{2\hbar^2}\sum_q C_q[\omega_A]\langle a_q^{\dagger}a_qS_{HO}+S_{HO}a_q^{\dagger}a_q-2\,a_q^{\dagger}S_{HO}a_q\rangle. \tag{A2}$$

In the particular case $S_{HO}=a_q$, and using the commutation relations between the creation and annihilation operators, Eq. (A2) yields the relaxation equation of the dipole amplitude

$$\left.\frac{d\langle a_q\rangle}{dt}\right|_{relax}=-\frac{\mathscr{D}_{HO}^2}{2\hbar^2}C_q[\omega_A]\langle a_q\rangle. \tag{A3}$$

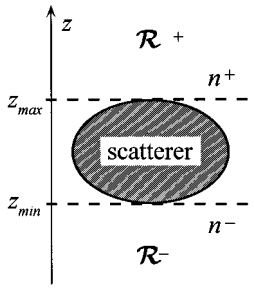

FIG. 11. Notations used.

Because of the property of the harmonic oscillator mentioned in Sec. II C 2 and demonstrated in [9], this evolution equation can be cast in the same form as the damping equation of the corresponding classical harmonic oscillator. Thus, one also has

$$\left.\frac{d\langle a_q\rangle}{dt}\right|_{relax} = -\frac{\Gamma_q}{2}\langle a_q\rangle, \tag{A4}$$

where Γ_q is the damping rate of a *classical* oscillating dipole of polarization $\mathbf{u}_q$. By comparing Eqs. (A3) and (A4), it is thus possible to express the correlation functions of the quantum electric field in terms of two damping rates, $\Gamma_\parallel = \Gamma_{-1} = \Gamma_1$ and $\Gamma_\perp = \Gamma_0$, corresponding respectively to classical dipoles polarized parallel and orthogonal to the $z=0$ plane [12]

$$C_{\parallel,\perp}[\omega_A] = \frac{\hbar^2}{\mathscr{D}_{HO}^2}\Gamma_{\parallel,\perp}; \tag{A5}$$

hence Eq. (23).

APPENDIX B: DERIVATION OF THE FORMULA (55)

The method presented in Sec. III B 1 for calculating dipole radiation patterns and damping rates relies on Eq. (55). We demonstrate how this formula can be derived from Lorentz's reciprocity theorem [23]. We start by establishing some general results concerning the scattering of scalar wave fields by any linear scatterer embedded between two lossless dielectric media of refractive indices n^+ and n^-. Following Ref. [23], generalized reflection and transmission coefficients for backward- and forward-scattered fields are introduced (Sec. II B 1), and are shown to satisfy a reciprocity relation, which generalizes the one introduced in [23] for the particular case $n^+ = n^- = 1$ (Sec. II B 2). Finally, this reciprocity relation is used for deriving Eq. (55) (Sec. II B 3).

1. Generalized transmission and reflection coefficients

We consider a monochromatic scalar field $E_{in}(\mathbf{r},t) = U_{in}(\mathbf{r})\exp(-i\omega t)$ incident upon a linear scatterer situated within the strip $z_{\min} \leqslant z \leqslant z_{\max}$. The strip is surrounded by two lossless dielectric media of refractive indices n^+ (half-space $z > z_{\max} \equiv \mathscr{R}^+$) and n^- (half-space $z < z_{\min} \equiv \mathscr{R}^-$) (see Fig. 11). This situation includes, for example, the one considered in this paper where the scatterer consists of the multilayered dielectric medium *and* the classical dipole, $n^+ = 1$, and where n^- is the refractive index of the lower-lying dielectric layer. We denote by $U_s(\mathbf{r})$ the spatial part of the scattered field, the time dependence of which is also $\exp(-i\omega t)$. The total field U is, of course, the sum of the incident and the scattered fields.

It is well known that under very general conditions the total field in each of the two half-spaces may be represented in the form of an angular spectrum of plane waves, both homogeneous and evanescent [25]. However, since we are interested only in the fields far from the scatterer, we can omit the contribution of evanescent waves, and the total field can be written as, in $\mathscr{R}^-$:

$$U(\mathbf{r}) = -\frac{ik^-}{2\pi}\int_{\sigma^{(+)}} C^{(-)}(\mathbf{n})\exp(ik^-\mathbf{n}\cdot\mathbf{r})d\Omega + \frac{ik^-}{2\pi}\int_{\sigma^{(-)}} D^{(-)}(\mathbf{n})\exp(ik^-\mathbf{n}\cdot\mathbf{r})d\Omega, \tag{B1a}$$

and in $\mathscr{R}^+$:

$$U(\mathbf{r}) = -\frac{ik^+}{2\pi}\int_{\sigma^{(-)}} C^{(+)}(\mathbf{n})\exp(ik^+\mathbf{n}\cdot\mathbf{r})d\Omega + \frac{ik^+}{2\pi}\int_{\sigma^{(+)}} D^{(+)}(\mathbf{n})\exp(ik^+\mathbf{n}\cdot\mathbf{r})d\Omega. \tag{B1b}$$

In Eqs. (B1), $\mathbf{n} \equiv (n_x, n_y, n_z)$ are unit vectors, $k^\pm = n^\pm\omega/c$ are the wave vectors associated with the frequency ω in half-space $\mathscr{R}^\pm$ (c being the speed of light *in vacuo*), $d\Omega = \sin\theta d\theta d\varphi$ is the element of solid angle generated by the unit vector $\mathbf{n}$, and $\sigma^{(+)}$ and $\sigma^{(-)}$ are unit hemispheres in $\mathbf{n}$ space defined as

$$\sigma^{(+)}: \quad n_z \geqslant 0, \tag{B2a}$$

$$\sigma^{(-)}: \quad n_z < 0. \tag{B2b}$$

The factors $C^{(\pm)}(\mathbf{n})$ and $D^{(\pm)}(\mathbf{n})$ have the physical significance of amplitudes of homogeneous plane waves that propagate in different directions either toward the scatterer [waves with amplitudes $C^{(+)}(\mathbf{n})$ and $C^{(-)}(\mathbf{n})$], or away from it [waves with amplitudes $D^{(+)}(\mathbf{n})$ and $D^{(-)}(\mathbf{n})$]. However, they also have another physical significance, which becomes evident when one examines the behavior of the total field far from the scatterer. One then finds that as the distance r of the field point from the origin (taken within the scatterer) increases along any direction specified by the unit vector $\mathbf{u}$ [23]

$$U(r\mathbf{u}) \sim C^{(\pm)}(-\mathbf{u})\frac{\exp(-ik^\pm r)}{r} + D^{(\pm)}(\mathbf{u})\frac{\exp(ik^\pm r)}{r}, \tag{B3}$$

where the plus or minus signs are taken on the right-hand side according to whether the field point $\mathbf{r} = r\mathbf{u}$ is located in the half-space $\mathscr{R}^+$ or $\mathscr{R}^-$, respectively. Equation (B3) expresses the far field in each of the two half-spaces as the sum of a convergent and a divergent spherical wave with complex amplitudes $C^{(\pm)}$ and $D^{(\pm)}$. This result implies that the integrals in Eqs. (B1) that contain the spectral amplitudes $C^{(\pm)}$ represent a field that is *incoming* at infinity, whereas the in-

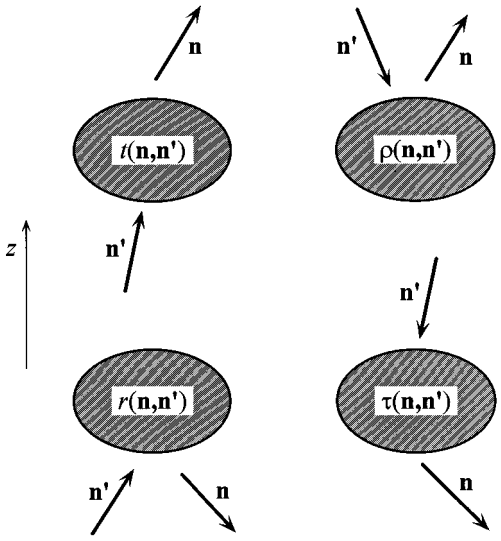

FIG. 12. Significance of t, ρ, τ, and r as generalized transmission and reflection coefficients.

tegrals containing the spectral amplitudes $D^{(\pm)}$ represent a field that is *outgoing* at infinity.

Finally, following [23] we define generalized transmission (t, τ) and reflection (r, ρ) coefficients through the relations (see Fig. 12)

$$D^{(+)}(\mathbf{n}) = -n^-/n^+ \int_{\sigma^{(+)}} t(\mathbf{n},\mathbf{n}')C^{(-)}(\mathbf{n}')d\Omega' - \int_{\sigma^{(-)}} \rho(\mathbf{n},\mathbf{n}')C^{(+)}(\mathbf{n}')d\Omega', \tag{B4a}$$

$$D^{(-)}(\mathbf{n}) = -\int_{\sigma^{(+)}} r(\mathbf{n},\mathbf{n}')C^{(-)}(\mathbf{n}')d\Omega' - n^+/n^- \int_{\sigma^{(-)}} \tau(\mathbf{n},\mathbf{n}')C^{(+)}(\mathbf{n}')d\Omega', \tag{B4b}$$

where the minus signs and the refractive index ratios in front of the integrals are included so that t, τ, r, and ρ are directly related to the usual transmission and reflection Fresnel coefficients at the interface between the half-spaces $\mathscr{R}^+$ and $\mathscr{R}^-$ in the absence of scatterer, as expected physically. These generalized coefficients are defined only for the following ranges of the z components of the unit vectors $\mathbf{n}$ and $\mathbf{n}'$

$$t(\mathbf{n},\mathbf{n}'): \quad n_z>0, \quad n_z'>0, \tag{B5a}$$

$$r(\mathbf{n},\mathbf{n}'): \quad n_z<0, \quad n_z'>0, \tag{B5b}$$

$$\tau(\mathbf{n},\mathbf{n}'): \quad n_z<0, \quad n_z'<0, \tag{B5c}$$

$$\rho(\mathbf{n},\mathbf{n}'): \quad n_z>0, \quad n_z'<0. \tag{B5d}$$

2. Reciprocity relations

Consider Lorentz's reciprocity theorem for scalar fields [23]

$$\int_\sigma \mathbf{J}(r\mathbf{n})\cdot\mathbf{n}dS = 0, \tag{B6}$$

where $dS = r^2 d\Omega$ and the integration is extended to a sphere σ of infinite radius, $\mathbf{n}$ being the local outward normal to this surface. The vectorial quantity $\mathbf{J}$ in Eq. (B6) is given by

$$\mathbf{J} = U_2\nabla U_1 - U_1\nabla U_2 \tag{B7}$$

with U_1 and U_2 two arbitrary solutions of the Helmoltz equation

$$\nabla^2 U + k^2 U = F(\mathbf{r})U, \tag{B8}$$

$F(\mathbf{r})$ being the scattering potential of the scatterer [for example, for a multilayered dielectric medium *alone* characterized by the spatial refractive index variation $n(z)$, $F(\mathbf{r}) = -k^2(n^2(z)-1)$]. It is important to note that this theorem holds irrespective of whether $F(\mathbf{r})$ is absorbing or not [23]. In particular, all the results obtained in this paper would apply identically in situations where some dielectric layers (except the outermost ones) have *complex* refractive indices. The integral in Eq. (B6) can be transformed by distinguishing between the contributions of the hemispheres $\sigma^{(+)}$ and $\sigma^{(-)}$. This yields

$$\int_{\sigma^{(+)}} \mathbf{J}^{(+)}(r\mathbf{n})\cdot\mathbf{n}d\Omega + \int_{\sigma^{(-)}} \mathbf{J}^{(-)}(r\mathbf{n})\cdot\mathbf{n}d\Omega = 0 \tag{B9}$$

with $\mathbf{J}^{(\pm)}$ defined in $\mathscr{R}^\pm$ as

$$\mathbf{J}^{(\pm)} = U_2^{(\pm)}\nabla U_1^{(\pm)} - U_1^{(\pm)}\nabla U_2^{(\pm)}. \tag{B10}$$

By substituting into Eq. (B9) the asymptotic form of the field U given by Eq. (B3), then replacing the amplitudes D by means of the relations (B4), and making use of the arbitrariness of U_1 and U_2, it is straightforward to show that the Lorentz theorem (B9) yields the following reciprocity relations between the generalized transmission and reflection coefficients:

$$n^- t(-\mathbf{n}',-\mathbf{n}) = n^+\tau(\mathbf{n},\mathbf{n}'), \tag{B11a}$$

$$n^+\tau(-\mathbf{n}',-\mathbf{n}) = n^- t(\mathbf{n},\mathbf{n}'), \tag{B11b}$$

$$\rho(-\mathbf{n}',-\mathbf{n}) = \rho(\mathbf{n},\mathbf{n}'), \tag{B11c}$$

$$r(-\mathbf{n}',-\mathbf{n}) = r(\mathbf{n},\mathbf{n}'). \tag{B11d}$$

3. Calculation of dipole radiation patterns

We now return to the problem of radiation by a classical dipole in the vicinity of a dielectric medium. We first note that this problem is equivalent to scattering of an incident wave by the system consisting of the dielectric medium and an anisotropically polarizable system (the polarized dipole). Second, we remark that as far as the radiation patterns $\mathscr{P}_{\parallel,\perp}^{s,p}(\theta) = P_{\parallel,\perp}^{s,p}(\theta,\psi_{\parallel,\perp}^{s,p})$ are concerned [the value of the azimuthal angle $\psi_{\parallel,\perp}^{s,p}$ can be readily infered from the definition of $\mathscr{P}_{\parallel,\perp}^{s,p}(\theta)$ given in Sec. III B 1], this process clearly belongs to scalar scattering theory, provided the incoming fields used in calculating $\mathscr{P}_{\parallel,\perp}^{s,p}(\theta)$ are chosen with the appropriate polarizations and azimuthal angles of propagation

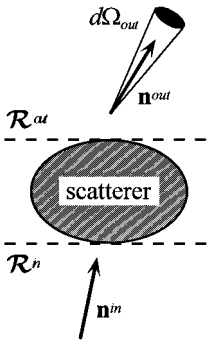

FIG. 13. Notations used.

(this is assumed throughout). This makes it legitimate, on the one hand, to drop the subscripts $\|,\perp$ and the superscripts s, p in the expressions for the fields and radiated powers, and, on the other hand, to make use of the results obtained in the preceding sections B 1, B 2, and of the reciprocity relations (B11) in particular.

Following the preceding remarks, we consider a plane wave of amplitude $\mathscr{E}_{in}$ incident from the half-space $\mathscr{R}^{in=\pm}$ and propagating in the direction of the unit vector $\mathbf{n}_{in=\pm}$ belonging to the hemisphere $\sigma^{(-in)}$ scattered into the solid angle $d\Omega_{out}$ generated by the unit vector $\mathbf{n}_{out=\pm}$ belonging to the hemisphere $\sigma^{(out)}$ (see Fig. 13). In order to connect the incident and scattered fields by means of the generalized transmission and reflection coefficients (see Sec. B 1), we first express the incident field in the form

$$U_{in}(\mathbf{r})=\mathscr{E}_{in}\exp(ik^{in}\mathbf{n}_{in}\cdot\mathbf{r}) =\mathscr{E}_{in}\int_{\sigma^{(-in)}}\Delta(\mathbf{n}-\mathbf{n}_{in})\exp(ik^{in}\mathbf{n}\cdot\mathbf{r})d\Omega, \tag{B12}$$

where $\Delta(\mathbf{n}-\mathbf{n}_{in})$ is the spherical Dirac delta function defined by the formula [23]

$$\Delta(\mathbf{n}-\mathbf{n}_{in})=\frac{\delta(\theta-\theta_{in})\delta(\varphi-\varphi_{in})}{|\sin\theta|} \tag{B13}$$

and δ is the usual one-dimensional Dirac delta function. Second, we make use of the asymptotic form ($k^{out}r\to\infty$) of the outgoing part of the field scattered into the direction $\mathbf{n}_{out}$ [see Eq. (B3)],

$$U_s(r\mathbf{n}_{out})\sim D^{(out)}(\mathbf{n}_{out})\frac{\exp(ik^{out}r)}{r}, \tag{B14}$$

to express the power $\Pi_{out}(\mathbf{n}_{out})d\Omega_{out}$ radiated by the scatterer in the solid angle $d\Omega_{out}$

$$\Pi_{out}(\mathbf{n}_{out})=n^{out}|D^{(out)}(\mathbf{n}_{out})|^2. \tag{B15}$$

Finally, by combining Eqs. (B12), (B1), (B4), and (B15), we obtain

$$\Pi_{out}(\mathbf{n}_{out})=\frac{\lambda^2}{n^{out}}|a(\mathbf{n}_{out},\mathbf{n}_{in})\mathscr{E}_{in}|^2, \tag{B16}$$

where $\lambda=2\pi\omega/c$ is the optical wavelength and (see Fig. 13)

$$a(\mathbf{n}_{out=+},\mathbf{n}_{in=-})=t(\mathbf{n}_{out},\mathbf{n}_{in}), \tag{B17a}$$

$$a(\mathbf{n}_{out=-},\mathbf{n}_{in=-})=r(\mathbf{n}_{out},\mathbf{n}_{in}), \tag{B17b}$$

$$a(\mathbf{n}_{out=-},\mathbf{n}_{in=+})=\tau(\mathbf{n}_{out},\mathbf{n}_{in}), \tag{B17c}$$

$$a(\mathbf{n}_{out=+},\mathbf{n}_{in=+})=\rho(\mathbf{n}_{out},\mathbf{n}_{in}). \tag{B17d}$$

It is well known that the damping of an oscillating dipole can be interpreted as arising from the work of the dipole on the field exactly at its location. In other words, the total power radiated by the dipole is proportional to the imaginary part of its effective polarizability $\alpha_{eff}(Z)$ (which includes the influence of the dielectric medium, i.e., the back action resulting from field reflection) multiplied by the field intensity $|\mathscr{E}_{dip}(Z)|^2$ at the dipole location. We can therefore express the power radiated by the scatterer into the solid angle $d\Omega_{out}$ in terms of the normalized dipole radiation distribution $\mathscr{P}(\theta)$ as

$$\Pi_{out}(\mathbf{n}_{out})=\beta\ \mathrm{Im}(\alpha_{eff})L(-\mathbf{n}_{in})|\mathscr{E}_{in}|^2\mathscr{P}(\mathbf{n}_{out}), \tag{B18}$$

where β is a constant and where the Z-dependent coefficient L is defined as in Eqs. (54). By combining Eqs. (B16) and (B18), one then obtains

$$\frac{\lambda^2}{n^{out}}|a(\mathbf{n}_{out},\mathbf{n}_{in})|^2=\beta\ \mathrm{Im}(\alpha_{eff})L(-\mathbf{n}_{in})\mathscr{P}(\mathbf{n}_{out}), \tag{B19}$$

which is valid *for any choice of* $\mathbf{n}_{in}$ *and* $\mathbf{n}_{out}$. In particular, one can choose

$$\frac{\lambda^2}{n^{in}}|a(-\mathbf{n}_{in},-\mathbf{n}_{out})|^2=\beta\ \mathrm{Im}(\alpha_{eff})L(\mathbf{n}_{out})\mathscr{P}(-\mathbf{n}_{in}). \tag{B20}$$

We now divide Eq. (B19) by Eq. (B20), and use the relation

$$\frac{|a(\mathbf{n}_{out},\mathbf{n}_{in})|}{|a(-\mathbf{n}_{in},-\mathbf{n}_{out})|}=\frac{n^{out}}{n^{in}} \tag{B21}$$

derived from Eqs. (B17) and the reciprocity relations (B11). This yields

$$\frac{\mathscr{P}(\mathbf{n}_{out})}{n^{out}L(\mathbf{n}_{out})}=\frac{\mathscr{P}(-\mathbf{n}_{in})}{n^{in}L(-\mathbf{n}_{in})} \tag{B22}$$

or equivalently

$$\frac{\mathscr{P}(\theta_{out})}{n(\theta_{out})L(\theta_{out})}=\frac{\mathscr{P}(\theta_{in})}{n(\theta_{in})L(\theta_{in})}, \tag{B23}$$

where $n(\theta)$ is defined as in Sec. III B 1. Because the equality in Eq. (B23) holds whatever the angles θ_{in} and θ_{out}, we find that the radiation pattern $\mathscr{P}(\theta)$ is necessarily of the form

$$\mathscr{P}(\theta)=\kappa n(\theta)L(\theta), \tag{B24}$$

where κ is a real parameter independent of θ but possibly dependent on Z. As can be readily checked by considering values of θ close to π, for which $\mathscr{P}(\theta)$ simply represents the

transmission of free-space dipole radiation through the dielectric medium [22], the parameter κ is found to be independent of Z and equal to the constant $3/8\pi$, hence formula (55).

APPENDIX C: $L_{\parallel,\perp}^{s,p}(\theta)$ COEFFICIENTS FOR A SINGLE DIELECTRIC MEDIUM

We derive the $L_{\parallel,\perp}^{s,p}(\theta)$ coefficients for a classical dipole in vacuum located a distance Z above a single dielectric medium of refractive index n_2. Referring to Eqs. (54), $\mathscr{E}_{in}$ is incident from above when $0 \leqslant \theta < \pi/2$, and from below when $\pi/2 < \theta \leqslant \pi$. In the former case, $\mathscr{E}_{in}$ is both directly incident on the dipole and indirectly incident after a reflection off the vacuum-dielectric interface. In the latter case, $\mathscr{E}_{in}$ is incident on the dipole only after a transmission through the interface. Considering the more general case of an interface between two dielectric media of indices n_1 and n_2, the pertinent Fresnel reflection and transmission coefficients for s and p modes are, respectively,

$$\rho_{12}^{s}=\frac{n_1\cos\theta_1-n_2\cos\theta_2}{n_1\cos\theta_1+n_2\cos\theta_2}, \tag{C1a}$$

$$\rho_{12}^{p}=\frac{n_2\cos\theta_1-n_1\cos\theta_2}{n_2\cos\theta_1+n_1\cos\theta_2}, \tag{C1b}$$

$$t_{21}^{s}=\frac{2n_2\cos\theta_2}{n_1\cos\theta_1+n_2\cos\theta_2}, \tag{C1c}$$

$$t_{21}^{p}=\frac{2n_2\cos\theta_2}{n_2\cos\theta_1+n_1\cos\theta_2}, \tag{C1d}$$

where θ_1 and θ_2 are related by

$$n_1\sin\theta_1=n_2\sin\theta_2. \tag{C2}$$

In our case $n_1=1$, and we identify the regions

$$\text{(I):}\quad 0\leqslant\theta\leqslant\pi/2, \tag{C3a}$$

$$\text{(II):}\quad \pi/2\leqslant\theta\leqslant\pi-\theta_c, \tag{C3b}$$

$$\text{(III):}\quad \pi-\theta_c\leqslant\theta\leqslant\pi, \tag{C3c}$$

where

$$\sin\theta_c=1/n_2 \tag{C4}$$

defines the so-called critical angle. A straightforward calculation then obtains:

$$\text{(I):}\quad L_{\parallel}^{s}(\theta)=|1+\rho_{12}^{s}\exp(2ikZ\cos\theta)|^2, \tag{C5a}$$

$$\text{(II):}\quad L_{\parallel}^{s}(\theta)=|t_{21}^{s}|^2\exp(-2kZ\sqrt{n^2\sin^2\theta-1}), \tag{C5b}$$

$$\text{(III):}\quad L_{\parallel}^{s}(\theta)=|t_{21}^{s}|^2, \tag{C5c}$$

$$\text{(I):}\quad L_{\parallel}^{p}(\theta)=|1+\rho_{12}^{p}\exp(2ikZ\cos\theta)|^2\cos^2\theta, \tag{C6a}$$

$$\text{(II):}\quad L_{\parallel}^{p}(\theta)=|t_{21}^{p}|^2\exp(-2kZ\sqrt{n^2\sin^2\theta-1})\cos^2\theta, \tag{C6b}$$

$$\text{(III):}\quad L_{\parallel}^{p}(\theta)=|t_{21}^{p}|^2\cos^2\theta, \tag{C6c}$$

$$\text{(I):}\quad L_{\perp}^{p}(\theta)=|1+\rho_{12}^{p}\exp(2ikZ\cos\theta)|^2\sin^2\theta, \tag{C7a}$$

$$\text{(II):}\quad L_{\perp}^{p}(\theta)=|t_{21}^{p}|^2\exp(-2kZ\sqrt{n^2\sin^2\theta-1})\sin^2\theta, \tag{C7b}$$

$$\text{(III):}\quad L_{\perp}^{p}(\theta)=|t_{21}^{p}|^2\sin^2\theta, \tag{C7c}$$

where $\theta_1=\theta$ in region I and $\theta_2=\pi-\theta$ in regions II and III.

APPENDIX D: CALCULATION OF $L_{\parallel,\perp}^{s,p}(\theta)$ COEFFICIENTS FOR A DIELECTRIC WAVEGUIDE

The calculation of $L_{\parallel,\perp}^{s,p}(\theta)$ for a single interface (Appendix C) can readily be extended to the case of multiple interfaces [5]. For example, in going from one interface to two interfaces (medium 2 bounded), the pertinent Fresnel reflection and transmission coefficients become

$$\rho_{123}=\frac{\rho_{12}+\rho_{23}\exp(2i\beta_2)}{1+\rho_{12}\rho_{23}\exp(2i\beta_2)}, \tag{D1a}$$

$$t_{321}=\frac{t_{32}t_{21}\exp(i\beta_2)}{1+\rho_{32}\rho_{21}\exp(2i\beta_2)}, \tag{D1b}$$

where $\beta_i=\omega/cn_il_i\cos\theta_i$, and l_i is the thickness of medium i. By iteration, this can be extended to three interfaces, appropriate for a waveguide geometry (media 2 and 3 bounded). Taking care in the iteration sequence, one finds

$$\rho_{1234}=\frac{\rho_{12}+\rho_{234}\exp(2i\beta_2)}{1+\rho_{12}\rho_{234}\exp(2i\beta_2)}, \tag{D2a}$$

$$t_{4321}=\frac{t_{43}t_{321}\exp(i\beta_3)}{1+\rho_{43}\rho_{321}\exp(2i\beta_3)}. \tag{D2b}$$

We note that Eqs. (D1) and (D2) are valid for both *TE* and *TM* modes provided they are traced back to the appropriate single interface coefficients [Eqs. (C1)]. Proceeding then along the same lines as in Appendix C, the calculation of $L_{\parallel,\perp}^{s,p}(\theta)$ for a waveguide geometry is straightforward.

[1] M. Oria, M. Chevrollier, D. Bloch, M. Fichet, and M. Ducloy, Europhys. Lett. **14**, 527 (1991); see also M. Chevrollier, M. Fichet, M. Oria, G. Rahmat, D. Bloch, and M. Ducloy, J. Phys. (France) II **2**, 631 (1992), and references therein.

[2] See, for example, V. I. Balykin and V. S. Letokhov, Phys. Today **62**(6), 23 (1989); Appl. Phys. B **54** (1992), special issue on optics and interferometry with atoms; J. Phys. (Paris) **4** (1994), special issue on optics and interferometry with atoms.

[3] R. J. Cook and R. K. Hill, Opt. Commun. **43**, 258 (1982).

[4] T. Esslinger, M. Weidemüller, A. Hemmerich, and T. W.

Hänsch, Opt. Lett. **18**, 450 (1993); S. Feron, J. Reinhardt, S. Le Boiteux, O. Gorceix, J. Baudon, M. Ducloy, J. Robert, C. Miniatura, S. Nic Chormaic, H. Haberland, and V. Lorent, Opt. Commun. **102**, 83 (1993).

[5] R. Kaiser, Y. Lévy, N. Vansteenkiste, A. Aspect, W. Seifert, D. Leipold, and J. Mlynek, Opt. Commun. **104**, 234 (1994).

[6] See, for example, J. Hilgevoord, *Dispersion Relations and Causal Description* (North-Holland, Amsterdam, 1960).

[7] C. Cohen-Tannoudji, in *Les Houches, Session XXVII, 1975—Frontiers in Laser Spectroscopy*, edited by R. Balian, S. Haroche, and S. Liberman (North-Holland, Amsterdam, 1977), p. 28.

[8] G. Barton, Proc. R. Soc. London Ser. A **410**, 141 (1987); **410**, 175 (1987).

[9] J.-M. Courty and S. Reynaud, Phys. Rev. A **46**, 2766 (1992).

[10] Note that we have neglected the variation of the vacuum fluctuation spectrum on the scale of the interface-induced modification of the atomic resonance frequency. In the situations of experimental interest, this is legitimate as long as the distance between the atom and the interface is much larger than the atomic radius.

[11] For a discussion of these different viewpoints see, for example, J. Dalibard, J. Dupont-Roc, and C. Cohen-Tannoudji, J. Phys. (France) **43**, 1617 (1982).

[12] At a somewhat deeper level, Eq. (A5) is a direct consequence of the fluctuation dissipation relation in the vacuum state of the field: the damping rates of a harmonic dipole are indeed proportional to commutators of the electromagnetic field at the dipole position.

[13] M. Fichet, F. Schuller, D. Bloch, and M. Ducloy, Phys. Rev. A **51**, 1553 (1995).

[14] F. Zhou and L. Spruch, Phys. Rev. A **52**, 297 (1995).

[15] Note that the van der Waals interaction potential can also be readly derived taking the electrostatic limit ($c \to \infty$) of Eq. (4.14) in Ref. [14]. We have checked that both methods yield identical results.

[16] S. Haroche, in *Fundamental Systems in Quantum Optics*, Les Houches session LIII, edited by J. Dalibard, J. M. Raimond, and J. Zinn-Justin (Elsevier, New York, 1992).

[17] J. D. Jackson, *Classical Electrodynamics* (Wiley, New York, 1975), p. 147.

[18] A. Lindgård and S. E. Nielsen, At. Data Nucl. Data Tables **19**, 533 (1977).

[19] A. Messiah, *Quantum Mechanics* (North-Holland, Amsterdam), Vol. II, p. 1077.

[20] A. Sommerfeld, Ann. Phys. (Leipzig) **28**, 665 (1909); **81**, 1135 (1926); *Partial Differential Equations of Physics* (Academic Press, New York, 1949).

[21] R. R. Chance, A. Prock, and R. Silbey, *Advances in Chemical Physics*, edited by I. Prigogine and S. A. Rice (Wiley, New York, 1978), Vol. XXXVII, p. 1.

[22] W. Lukosz and R. E. Kunz, J. Opt. Soc. Am. **67**, 1607 (1977); **67**, 1615 (1977); W. Lukosz, *ibid.* **69**, 1495 (1979).

[23] M. Nieto-Vesperinas, *Scattering and Diffraction in Physical Optics* (Wiley, New York, 1991), Chap. 5; see also M. Nieto-Vesperinas and E. Wolf, J. Opt. Soc. Am. A **3**, 2038 (1986).

[24] J. D. Jackson, *Classical Electrodynamics* (Wiley, New York, 1975), p. 278.

[25] E. Wolf, Proc. Phys. Soc. London **74**, 269 (1959).